[Frontiers in Bioscience 13, 1281-1293, January 1, 2008]

Overview of bioluminescence tomography-a new molecular imaging modality

Ge Wang[1], Wenxiang Cong[1], Haiou Shen[1], Xin Qian[1], Michael Henry[2], Yue Wang[3]

[1]Bioluminescence Tomography Laboratory, VT-WFU School of Biomedical Engineering and Sciences, Virginia Polytechnic Institute and State University, 1880 Pratt Drive, Suite 2000, MC-0493, Blacksburg, VA 24061, USA,[2]Department of Molecular Physiology and Biophysics, University of Iowa, 200 Hawkins Drive, Iowa City, IA 52242, USA,[3]Computational Bioinformatics and Bio-imaging Laboratory, Department of Electrical, Computer, and Biomedical Engineering, Virginia Polytechnic Institute and State University, Arlington, VA 22203, USA

TABLE OF CONTENTS

1. ABSTRACT

According to the NIH roadmap (1), optical molecular imaging has an instrumental role in the development of molecular medicine. Great efforts, including those with bioluminescent imaging techniques, have been made to understand the linkage between genes and phenotypic expressions in normal and disease biology. Currently, bioluminescent techniques are widely used in small animal studies. However, most of the current bioluminescent imaging techniques are done in the 2D mode. In this overview, we review bioluminescence tomography (3D mode), elaborate on its principle and multi-spectral extension, describe associated image unmixing and normalization techniques, and discuss a number of directions for technical improvements and biomedical applications.

2. INTRODUCTION

Molecular imaging is to study biological processes *in vivo* at the cellular and molecular levels. It may non-invasively differentiate normal from diseased states and monitor physiological processes especially therapeutic responses. More importantly, the imaging of molecular signatures, specific proteins and biological pathways allows *early* diagnosis and *individualized* therapies, an integral part of molecular medicine (2-4). While some classic techniques do reveal information on micro-structures of the tissues, only recently have molecular probes been developed along with imaging tools that are sensitive and specific for detecting molecular targets in animals and humans. Among molecular imaging modalities (5-14), optical imaging has attracted a remarkable attention for its unique advantages, especially

excellent performance, radiation-free and cost-effectiveness. Fluorescent and bioluminescent probes are commonly used for optical molecular imaging. Today, fluorescent and bioluminescent imaging techniques are most widely applied in mouse studies

Among various optical molecular imaging techniques, fluorescence molecular tomography (FMT) (15, 16) and bioluminescence tomography (BLT) (17-19) are two complementary modes. FMT was developed by Ntziachristos *et al.*, in which fluorescence reporters (molecular beacons, tagging agents, fluorescent proteins) are reconstructed in a mouse. FMT illuminates the animal from different orientations at the excitation wavelength and detects resultant optical signals using a CCD camera and filters. Then, a photon transport model is used to reconstruct the tagged sources. In contrast to fluorescent imaging which is complicated by auto-fluorescence, there is little or no background light source associated with bioluminescent imaging. The introduction of BLT relative to planar bioluminescent imaging can be, in a substantial sense, compared to the development of x-ray CT based on radiography. Without BLT, bioluminescent imaging is primarily qualitative or can only be quantitated by relative changes in signal intensity over time. With BLT, quantitative and localized analyses on a bioluminescent source distribution become feasible in a mouse, which reveal molecular and cellular signatures critically important for numerous biomedical studies and applications.

Since 2002, our team at University of Iowa has been working on BLT and recently demonstrated *in vivo* BLT results (16-18, 20-25). Here we provide an overview of BLT to outline the progress in this area, point out remaining obstacles and discuss possible solutions to these problems. In the next section, we review important ideas and results on bioluminescence tomography, elaborate on its multi-spectral extension, and cover both the system design and algorithm development. In the forth section, we describe associated image unmixing techniques. In the fifth section, we present the potential of temperature-modulated bioluminescent tomography techniques for superior reconstruction quality. In the sixth section, we discuss a number of directions for technical improvements and biomedical applications.

3. BIOLUMINESCENCE TOMOGRAPHY

In 2002, the first bioluminescence tomography (BLT) prototype was conceptualized. In 2003, the first BLT prototype was reported that compensates for heterogeneous scattering properties of a mouse and performs quantitative 3D reconstruction of internal sources from bioluminescent views measured on the external surface of the mouse (26). In this section, we outline the development and key results in this new area.

3.1. Precursory work

Generally speaking, luminescence means the emission of light by a substance caused by physical or chemical means including but not limited to *photoluminescence* by a light beam such as fluorescence, cathodoluminescence by an electron beam, thermoluminescence by heat, chemiluminescence from a chemical reaction, and *bioluminescence* from a biochemical enzyme-driven reaction in living organisms and animals. Berthold Technologies (http://www.berthold.com/ww/en/pub/bioanalytik/biomethods/luminescence.cfm) is a leader in luminescence measuring technology. Because of importance of bioluminescence imaging (BLI) and fluorescence imaging, in 1989 Berthold TechnologieS introduced the LB 980 Luminograph (27), which is its first low light imaging system. The first *in vivo* gene expression experiments in plants and animals were performed on this instrument in 1992 (28). Another company also early involved in BLI was Hamamatsu which had its Argus-50 system for imaging macro samples (29). Philip E. Stanley (30-33) reported in several surveys about instrumentation and reagents in BLI.

Dr. Contag's group at Stanford University made pioneering contributions in the BLI area (6, 34-36). The main idea is that biological light sources can be used to report externally the inner workings of mammalian biology and studies mice as models of human diseases. Although biological tissues are very diffusive, bioluminescent light may be detected after transmission of a few centimeters (37, 38). Based on these results, Xenogen Corporation (www.xenogen.com) was established to develop the bioluminescence imaging systems. The company received Frost and Sullivan's 2004 Award for Technology Innovation. The earlier Xenogen products are for planar bioluminescence imaging. Recently, they also developed the 3D bioluminescence imaging system based on the assumption that the mouse is optically homogeneous (39, 40). Hence, this system is currently not truly tomographic.

Our group at University of Iowa reported the first BLT system and initial feasibility results in the 2003 RSNA meeting (26, 41), which uses a CCD camera (Princeton Instruments VA 1300B, Roper Scientific, Trenton, NJ). Also, we performed a theoretical analysis on the solution uniqueness (17), which is actually the first paper in the field of bioluminescence tomography. To collect bioluminescent signals around a mouse, a stage is vertically rotated under computer control and horizontally moved by a transport to match the focal length of the camera. A holder maintains the position of the mouse, and clamps into the stage. A light-tight enclosure has an entry hatch to accommodate wires and minimize light leak. The front side of the box is removable for experimental manipulation of a mouse. Typically, for a given orientation two images are obtained with light on and off. Marks are placed on the mouse skin for registration with CT, MRI and diffuse optical tomography (DOT) scans of the same mouse. In contrast to the homogeneous mouse model based method, *the major advantage of the BLT approach* we pioneered is the capability of compensating for the heterogeneous optical attenuation maps within a mouse. In the early stage, we segmented a CT scan of a mouse into major anatomical regions, assigned optical parameters into each of the regions according to available data in the

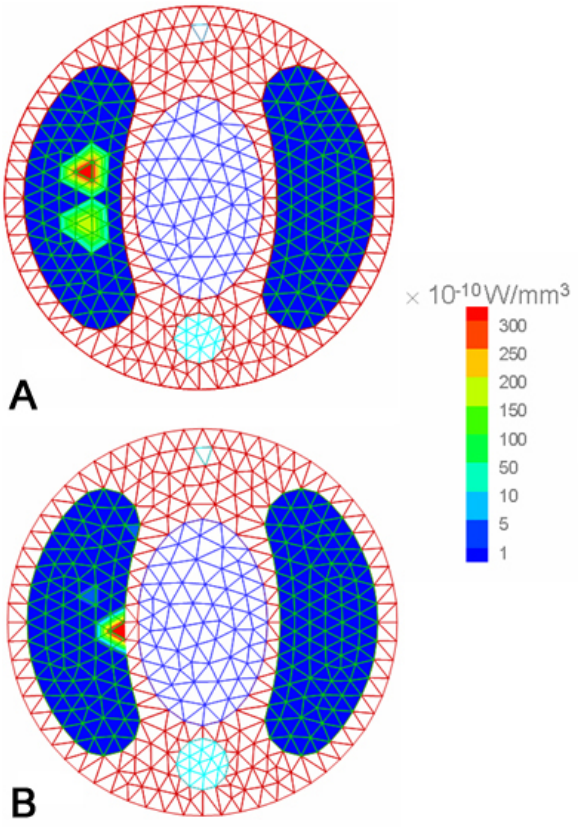

Figure 1. BLT validation with a physical phantom. (a) A finite-element reconstruction using our modality fusion approach, (b) the corresponding reconstruction incorrectly assuming that the phantom is homogeneous.

literature, and then performed BLT reconstructions. We have also recognized that *in vivo* DOT measurements in combination with the CT scan would produce better results, as discussed in the first author's talk for the Stanford 2005 MIPS/Philips Medical Molecular Imaging Seminar Series (http://mips.stanford.edu/public/mi_seminar05.adp).

3.2. Feasibility studies

Extensive studies were performed on theoretical analysis and image reconstruction (17, 42, 43), leading groups all suggest that BLT can produce valuable tomographic information in favorable cases or with strong *a priori* knowledge (17, 19, 37, 42, 44-49). For example, Wang *et al.* has so far developed two generations of BLT prototypes, which now produce 1-3mm accuracy in source localization and 10-30% error in source power estimation.

3.2.1. Phantom data

Cong *et al.* has fabricated a cylindrical heterogeneous tissue-simulating phantom (19). This phantom of 30mm height and 30mm diameter included four types of regions mimicking bone (B), heart (H), lung (L), and muscle/connective tissues (T). The optical parameters were measured using the DOT approach. It allows known bioluminescent/fluorescent sources (S) to be embedded in the middle cross-section. Two red luminescent liquid filled polythene tubes of 1mm height and 0.6mm diameter were placed inside the phantom at positions of 3mm separation on a central slice 17.5mm from the bottom. The phantom containing the two sources was put in the holder in front of the CCD camera, and went through the BLT data acquisition. Next, the pixel gray levels of the luminescent view were transformed into light units according to a calibration formula we established empirically. The BLT reconstruction was performed using the finite-element method. The finite-element model consisted of 7560 wedge elements and 4521 nodes. There were 11 circles separated by 0.975mm on the surface of the phantom, along each of which 64 detection locations were uniformly distributed. The results revealed that there were two light sources in the phantom located at (-8.67, 2.02, 17.9) and (-8.63, -2.02, 17.9)mm with total power densities of 3.10×10^{-8} and 1.85×10^{-8} watts/mm^3, respectively. The difference between the reconstructed and real source positions was within 1mm. The relative error of the reconstructed source strength was about 11.4% (19). On the other hand, as shown in Figure 1, when the phantom was assumed optically homogeneous with the average optical parameters, the reconstruction yielded only one source, which clearly indicates the general invalidity of the homogeneous mouse model based method.

3.2.2. *In vivo* data

In addition to the phantom experiment, Wang *et al.* also conducted mouse studies using a mouse model of prostate cancer metastasis based on intracardiac injection of tumor cells (50). In their model, luciferase-expressing tumor cells are introduced into the arterial circulation through the left cardiac ventricle. This allows seeding of tumor cells in bone, liver adrenal glands and other sites commonly involved in metastatic prostate cancer in humans. However, a key limitation of this model is that precise anatomical localization cannot be ascertained from conventional bioluminescence imaging. We used BLT to localize the sources as shown in Figure 2, in which the stronger source has a power of 39.8nano Watts (right), and the smaller one has a power of 1.5nano Watts (left) (50). Post-mortem analysis indicates that tumors were in both adrenal glands. Clearly, the reconstructed source positions were in excellent agreement with the actual locations of the tumors. On the other hand, the volume of tumor tissues as measured by Vernier calipers was 468mm^3 for the tumor on the right and 275mm^3 for the tumor on the left. Thus, there was a considerable discrepancy between the relative difference between the power measurements and tumor volumes. One possibility that shall be examined is whether the power values are better correlated with viable tumor tissue rather than tumor volume since tumor volume is a composite measurement of viable tumor cells (bioluminescent) and nonviable tumor cells as well as other components that are not bioluminescent.

3.3. Multi-spectral extension

A major topic in this area is multi-spectral bioluminescence tomography (MBT), which is a natural extension of the traditional single-spectral bioluminescence tomography (BLT) and covers the single-spectral counterpart as a special case. Here we underline that there

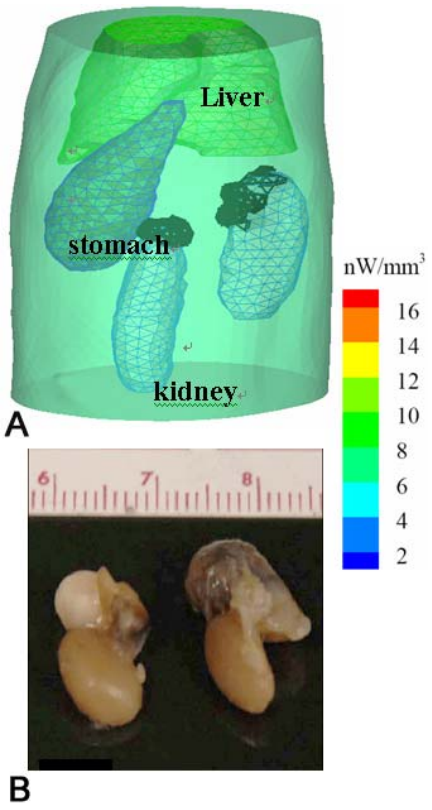

Figure 2. BLT and histological verification. (a) Two bioluminescent sources on the two kidneys, and (b) two tumors at the same locations on the dissected kidneys.

are two meanings attached to the concept of multi-spectral bioluminescence tomography (MBT). First, if we have only a single bioluminescent probe that is spatially and spectrally distributed, we can sample its spectrum into a number of bands or channels for multi-wavelength measurement, and then perform the probe source reconstruction (51, 52). To our best knowledge, the results on MBT by other groups so far were all done in this first sense (46, 47, 53). Second, when we use multiple bioluminescent probes that are spatially and spectrally distributed simultaneously, in addition to the multi-wavelength sampling and reconstruction, we shall further decompose their composite images into the individual components corresponding to the probe distributions in the light of known/pre-determined or concurrently estimated differential spectral-profiles (54-57).

While multi-spectral imaging as defined in the second sense has been reported in other applications especially *in vitro* fluorescent imaging (54-56), there are critical and immediate needs to differentiate spectral signatures in reconstructed images of *living mice* to recover multiple *in vivo* distributions of distinct bioluminescent probes. In this new context, the traditional *in vitro* assay can be advanced to *in vivo* imaging in small animal models. The Iowa team is currently working to *develop MBT in the above-defined second sense* to facilitate or enable mouse studies on complex biological processes and interactions labeled by multiple bioluminescent probes of different spectra. Using multiple target-seeking optical reporters in a single experiment, it is highly desirable and feasible to read out and unravel the composite molecular/cellular signatures of pathophysiologic events, even in tissues deep within a mouse body (54, 56).

The MBT system being developed in our Iowa group promises to improve the state of the art in the BLT area significantly. First, our MBT system design allows parallel acquisition of multi-view and multi-spectral data, which is the first of its kind and will minimize the effect of bioluminescent signal decay, improve signal-to-noise ratio, and increase system throughput dramatically. Second, the MBT images are decomposed using the composite-image unmixing methods, targeting the reconstruction of multiple bioluminescent probe distributions inside a living mouse, instead of being only limited to the reconstruction of a single probe distribution in 3D, for both completely and partially known spectra of bioluminescent probes. While spectral unmixing has been extensively studied over decades, image/signal unmixing in the cases of partially known spectra remains an open and challenging problem, which has been inspired by the elegant results in the area of blind source separation. Use of new unmixing techniques to be described in Appendix A is a significant novel feature of our proposed MBT system. Also, when we work on the proposed MBT for reconstruction of multiple bioluminescent probe distributions, we will at the same time improve the traditional BLT reconstruction as well.

3.4. System design

As shown in Figure 3, our MBT system will be prototyped as a rather different system compared to the existing BLT systems designed by other groups. There are five components in the MBT system: multi-view subsystem, multi-spectral subsystem, image acquisition subsystem, a diffuse optical tomography (DOT) subsystem (not shown in the figure) and a reconstruction engine. All the components shall be secured using mounts and holders inside a light-tight box.

3.4.1.Multi-view setup

We recently reported a prototype design at the Molecular Imaging meeting in Hawaii and are currently working to optimize this design. As shown in Figure 3, the multi-view subsystem will include a mounting plate, four mirror stages, and four mirrors. The aluminum mounting plate is a square of 24 cm side length and 10 mm thickness. The aluminum mirror stages are right-angle blocks of 10 cm side length and 3 cm thickness. The aluminum triangular blocks are mounted on the mounting plate symmetrically around the mouse, which is held in an optically transparent cylindrical (Syntec Tech. Inc.) mouse holder of radius 12.5 mm and length 10 cm. Four rectangular silver coating front mirrors (Thorlabs Inc.) of size 14×3 cm^2 are attached to each of the four hypotenuse surfaces of the mirror stages. The four views of the mouse in the mirrors are parallel to the mounting plate surface. If the mouse maintains in the center of the four mirrors, the four images of the mouse shall be in the same plane for the camera to focus on all of them simultaneously. To keep the

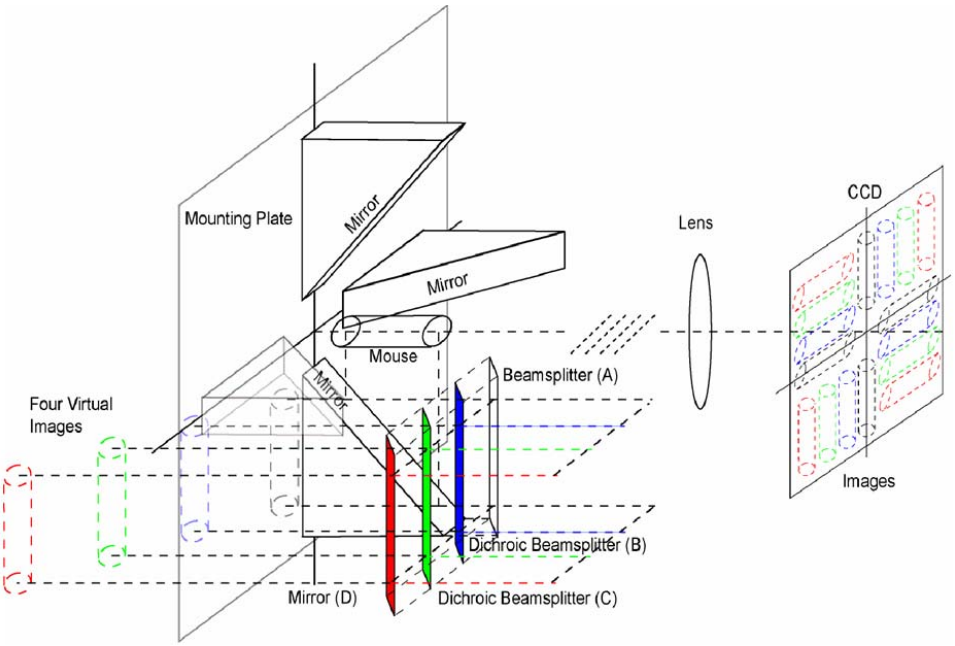

Figure 3. Proposed MBT system for parallel acquisition of multi-view multi-spectral data, including 4 mirrors in the selected wavelength ranges, a mouse holder, 4 beam splitters and 12 dichroic mirrors in corresponding spectral bands, a collimated lens and a CCD camera.

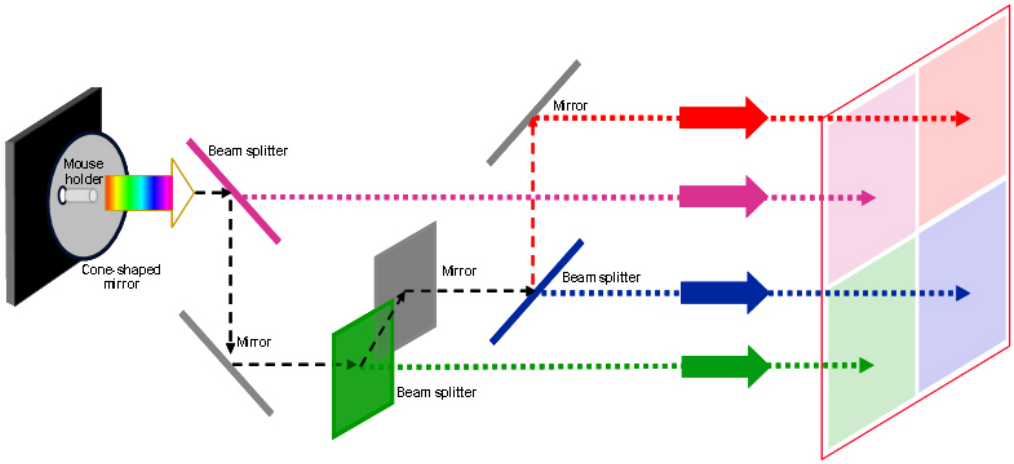

Figure 4. Design of a more sophisticated multi-spectral BLT system, which includes a CCD camera, a truncated cone-shaped mirror with a mouse holder on its principle axis, three beam splitters with different wavelength ranges and three highly reflective mirrors. The optical path differences can be optically corrected.

mouse holder in position, it can be attached to the mounting plate with an X-Y flexure stage, which can move the mouse holder within a 5mm range along each axis. Figure 4 shows our latest design of a more sophisticated multi-spectral BLT system, which includes a CCD camera, a truncated cone-shaped mirror with a mouse holder on its principle axis, three beam splitters with different wavelength ranges and three highly reflective mirrors. The optical path differences can be optically corrected. The merit of this system is to avoid photon leaking and utilize the detecting efficiently while keeping all the advantages we have with the previous design.

3.4.2.Multi-spectral setup

To equip the multi-view subsystem with a multi-spectral imaging capability, a multi-spectral subsystem shall be added in front of the multi-view subsystem. Since the four views of the multi-view subsystem are symmetric, we only need show the optical path for one view in Figure 3. A plane beam splitter (A) (Edmund Optics Inc.) splits the light emitted from mouse into two parts: 25% being directly transmitted to the CCD camera, and 75% reflected to a dichroic beam splitter (B) (Green-Red dichroic plate beam splitter, Edmund Optics Inc.). The dichroic beam splitter (B) reflects the signal in [530, 595]nm directly to

the CCD camera and transmits the rest light to another dichroic beam splitter (C) (Red-NIR dichroic plate beam splitter, Edmund Optics Inc.). The dichroic beam splitter (C) reflects the signal in [595, 664]nm to the CCD camera and transmits the signal in [664, 726]nm to a silver coating front mirror (D) (Thorlabs Inc.). The mirror (D) reflects the remaining spectrum to the CCD camera. All the beam splitters, dichroic beam splitters, and mirrors have the same size 10×5 cm^2. In Figure 3, there are four virtual images for each view, corresponding to multi-spectral data in [500, 750]nm, [530, 595]nm, [595, 664]nm and [664, 726]nm, respectively. Hence, we have in total 16 images on the CCD. There is one problem with this solution - the four spectral images are not on the same plane and thus cannot be focused on simultaneously. One simple solution is to use optical delay systems, which is technically straightforward.

3.4.3. Data acquisition

A highly sensitive CCD camera (Princeton Instruments VersArray 2048B) shall be used for image acquisition. It supports 2048×2048 imaging pixels, 13.5×13.5μm^2 pixel size, and a 16bits dynamic range. In the spectral range [500, 750]nm, quantum efficiency (QE) is higher than 80% (peak EQ > 92% at 550 nm). The camera can be cooled to -110^oC using the Cryotiger cooling device. At this temperature, the typical CCD read noise is 2 electrons rms, and the dark current is less than 1 electron per hour per pixel. The camera is coupled with a Nikon normal 50mm f/1.2 AIS manual focus lens (Nikon Inc.), and mounted on a travel stage to adjust the focal distance. The minimum focus distance is 50cm with a field of view 25×25 cm^2. Since the total area of the images can be made 24×24 cm^2, the system can cover all the multi-spectral signals in parallel.

The diffuse optical tomography (DOT) subsystem utilizes a tunable laser (TOPTICA Photonics AG) with 525-700nm wavelength range and average power of 10mW. A mirror system with rotation and translation ability scans the laser beam across the mouse surface. Then, the 4-views of diffusive signals around the mouse can be recorded on the CCD camera within a few minutes. The body surface of a mouse can be reconstructed from a CT scan. Finally, the optical properties of the mouse can be reconstructed (16). It is recognized that the DOT-based attenuation mapping is a critical step for BLT/MBT/FBT reconstructions, and our proposed DOT system does not take advantage of time-resolved measurements. Our approach may need to be improved in reference to the work on time-resolved DOT. Also, DOT can be performed utilizing micro-CT, micro-MRI and resultant atlases to improve the reconstruction quality. We have been using this multi-modality approach for the past several years (50) with satisfactory results.

3.4.4. System calibration

The CCD camera shall be calibrated to remove noise and systematic biases utilizing bias frames, dark frames, and flat frames. Bias frames compensate for read-out noise and interference from the computer. Dark frames measure the dark current readout of the CCD. Flat frames correct disfigurements of the light paths and the CCD chip. After the calibration, an absolute intensity calibration of the whole imaging system shall be conducted to estimate the signal brightness in physical unit (Watts/cm^2/sr). For that purpose, an absolutely calibrated 8-inch integrating sphere (Sphere Optics, Inc) will be used. A 4-inch sphere contains a tungsten lamp light source. A 6-position automated filter wheel with 5 filters (500nm, 550nm, 600nm, 650nm, 700nm) and a variable attenuator with a large dynamic range will be placed between the two spheres to select a particular wavelength and control the light level entering the 8-inch sphere. The 2-inch output aperture of the 8-inch sphere produces as low as 2.07×10^{-13} Watts/cm^2/sr in the spectral region of interest. By imaging this output aperture, the gray level of the CCD can be mapped into physical unit.

3.4.5. Signal-to-noise ratio analysis

The signal-to-noise ratio (SNR) of a camera system can be computed as:

$$SNR = \frac{S}{\sqrt{S + D \times t + N^2}} \quad (1)$$

where S is the signal per pixel in electrons, t is the integration time, D is the dark current (electrons/pixel/second), and N the CCD read noise (electrons rms/pixel). A typical way to increase SNR is to sum pixels before readout. A binning value of k means that a group of $k\times k$ pixels is combined to form one super-pixel and have $k\times k$ times the original signal and the dark current. The readout noise remains the same if we use the VersArray 2048B CCD on-chip binning. Hence, we have

$$SNR_{k^2} = \frac{S \times k^2}{\sqrt{S \times k^2 + D \times t \times k^2 + N^2}} \quad (2)$$

The trade-off of binning is spatial resolution. In our BLT reconstruction, the size of each finite element is ~1mm. Hence, each pixel corresponds to a square of ~0.12×0.12mm^2 on the mouse body surface. Therefore, we can use 8×8 binning to increase SNR.

In addition to increasing the binning size, there are other ways to increase SNR. By capturing multi-view and spectrally resolved signals in parallel, we have more flexibility to increase the integration time allowing the detection of weaker signals and simplifying problems related to bioluminescence signal decay. In each experiment, 5-20 minutes can be used according to the signal strength. We can use a lens with a larger aperture to increase the signal strength significantly. For example, an f/1.0 lens can increase the signal 7.8 times versus an f/2.8 lens. On the other hand, a larger aperture will reduce the depth of field and make the camera focusing more difficult. Taking all the pros and cons into account, we choose an on-shelf f/1.2 lens.

3.5. Image reconstruction

The mouse model is a key component for BLT/MBT image reconstruction. In this context, we consider that the mouse model includes (1) a physical

model of the photon migration, (2) a geometrical model of the mouse anatomy, and (3) optical parameters about properties of different mouse structures. In the following, we describe a novel technique for mouse modeling and image reconstruction to improve image quality, computational efficiency and numerical stability.

3.5.1 Physical modeling In bioluminescence imaging (BLI), the target cells emit bioluminescent photons under appropriate conditions. The bioluminescence signal includes a red region of the spectrum, permitting a significant penetration depth (34). Therefore a sufficiently large number of bioluminescent photons escape the attenuating environment, reach the body surface of a mouse, and can be detected using a highly sensitive CCD camera. The photon transmission in the biological tissue is subject to both scattering and absorption but the scattering predominates over the absorption. The propagation of bioluminescent photon in the biological tissue can be well described by the diffusion approximation model (58). The diffusion approximation model has been successfully applied for DOT, BLT and FMT.

3.5.2. Geometric modeling

A mouse can be scanned by micro-CT and/or micro-MRI for its anatomy. The acquired images can be segmented into major regions (heart, lungs, liver, muscle, spleen, and so on). We are also evaluating to what extent this process may be simplified using the mouse atlas deformable matching technique. Because the mouse anatomy is rather complex, it is difficult to reflect all the features in a geometrical model. Also, the numerical computation will become impractical given an overcomplicated geometrical model. Hence, one approach would be to segment an image volume into major organ regions approximately at ~0.5mm resolution. The commercial software *Amira* 4.1 (Mercury Computer Systems, Inc. Chelmsford, MA) is available for segmentation of images and construction of the mouse geometrical model. This will significantly simplify the geometric modeling. We acknowledge that there are differences between the geometrical model and the true mouse anatomy. However, in our mouse modeling process the optical parameters of the mouse can be optimally determined to compensate for the geometric mismatches.

3.5.3. Attenuation maps

Photon propagation in a mouse depends on not only the geometrical model but also the optical properties of the mouse. Based on the mouse geometrical model, *we consider the optical parameters (absorption, scattering coefficient, and anisotropic coefficient) as variables being piecewise constant within each organ region. Then, the optical parameters will be reconstructed in the spectral bands of interest using DOT.* In this procedure, the multi-excitation and multi-detection strategy shall be employed to enhance numerical stability. We typically use the finite element method for DOT (16). From the finite element theory, the diffusion equation and the boundary condition can be formulated into a finite-element-based matrix equation. An objective function is defined to measure the total variation between the model predicted photon density and measured photon density on the body surface of the mouse. The adjoint approach will be used as an effective and efficient way to calculate the gradient of the objective function (59). The Quasi-Newton method and an active set strategy will be used to solve the minimization problem subject to the simple constrains. Because the optical parameters are constrained to piecewise constant corresponding to different organ regions, the reconstruction of optical parameters will be numerically more robust, leading to an optimal mouse model for the purpose of MBT.

3.5.4. Source reconstruction

The diffusion equation and the boundary condition can be discretized into a set of finite-element-based matrix equations. Then, we can re-arrange the resultant equations and combine them into a set of linear equations in corresponding spectral bands. Then, the MBT reconstruction is transformed to find the source distributions in these bands at involved voxels such that the surface nodal flux densities $\Phi_1^{(k)}$ ($k = 1, 2, ..., N$) *computed* from the overall matrix system optimally match with the *measurement* $\Phi_{\text{meas}}^{(k)}$ when the target spectra of the involved bioluminescent probes are optimally satisfied. The real formulation is mathematically tedious, and will be omitted for brevity.

The unknown source density can be constrained within a permissible source region and an intensity range. In fact, the photon number emitted from a cell can be easily estimated in a bioluminescence imaging experiment, and the upper bound of the power emitted in an element can be approximated as the product of the number of cells in a finite element volume and the number of photons emitted from a cell. In addition, in bioluminescence imaging, high value clusters on bioluminescent views roughly indicate the source region. This prior knowledge can help define the permissible source region to reduce the number of unknown variables and enhance the stability of the MBT reconstruction. Accordingly, the reconstructed results can be optimized using an iterative procedure based on the gradually refined permissible region from earlier reconstruction results, as well as from coarser to finer meshes used for reconstruction.

4. TEMPERATURE MODULATION TECHNIQUE

Because the BLT is generally an ill-posed inverse source problem, it is highly desirable to regularize the solution and transform the source reconstruction into a better-conditioned setting. Zhao *et al.* recently reported that bioluminescent spectra can be significantly affected by temperature (60). Specifically, Luciferase enzymes from firefly (FLuc), click beetle (CBGr68, CBRed), and Renilla reniformins (hRLuc) have different emission spectra that are temperature dependent. Hence, the possibility of temperature-modulated bioluminescence tomography (TBT) is very attractive by utilizing focused ultrasound array as recently demonstrated in numerical simulation (61). Here we describe a more practical temperature-modulation technique for BLT/MBT.

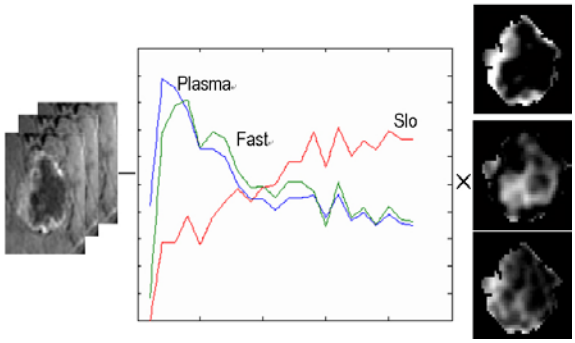

Figure 5. Latent variable modeling of 3-channel dynamic contrast-enhanced MRI. The reconstructed vascular permeability distributions are given in the right column. From top to bottom, the perfusion/diffusion categories include fast flow, slow flow, plasma input.

4.1. Temperature dependence of the bioluminescence signal

The temperature dependence of the bioluminescent spectra is an alternative mechanism for improving the BLT reconstruction. In a recent *in vivo* mouse study performed by our group in University of Iowa, temperature effects on the light intensity of the coleopteran luciferase Fluc were observed *in vivo*. A transgenic mouse with the Fluc expression throughout the body was placed on the temperature-adjustable stage in the bioluminescent imaging system IVIS 100 (Xenogen Corporation). The mouse body temperature was monitored constantly using a type T thermocouple thermometer (Cambell Scientific Inc.) inserted in the rectum. Because the normal mouse body temperature is about 37 ^{o}C and the body temperature will drop to ~25 ^{o}C when a mouse is anaesthetized, we did the temperature modulated experiments at these two settings. First, the stage was set at 25^{o}C, and the mouse was anesthetized by inhalation of isoflurane. When the mouse body temperature was stabilized ~24^{o}C, the thermometer was removed, and D-luciferin (150 mg/kg body weight, i.p. injection) was administered. After BLI for 34 minutes, the thermometer was put back to record the mouse body temperature 24.85 ^{o}C. During the BLI process, a series of images was acquired using each of the four filters (Open-filter, GFP 490-510nm, DsRed 558-583nm, Cy5.5 675-694nm). Images were collected with exposure time 0.5 second and a 20 cm field of view. The region of interest (ROI) was applied to the entire mouse. Light output from the ROI was quantified as the total number of photons emitted per second using the Living Image software (v2.5, Xenogen Corporation). As verified using the IVIS 100 system, there was no light emitted from the mouse after 3.5 hours from the end of the first experiment. Then, the second experiment was conducted on the same mouse. This time, the stage temperature was set to 40 ^{o}C, and the mouse body temperature maintained at ~37 ^{o}C. Then, the BLI was repeated using the same protocol. The mouse body temperature was recorded as 37.03 ^{o}C after BLI for 34 minutes. A plot of the flux measured against the time indicates a strong influence of temperature on luciferase enzyme kinetics and pharmacokinetics of the luciferin substrate, as shown in Figure 5.

4.2. Control of the mouse body temperature

Based on the above preliminary results, two bioluminescent datasets can be respectively collected at a relatively low base temperature (say, 25^{o}C) and a significantly elevated temperature (say, 37^{o}C) within the same mouse. An air-based temperature control device (SA Instruments, Inc.) can be employed to control the temperature within a dedicated mouse holder, which will in turn modulate the temperature distribution within the mouse subject to biocompatibility (≤40oC). This device can take room temperature air (25oC) into a heating module and brings the air to a target temperature (for example, 40oC). The heated air is used to keep the mouse at a desirable temperature level, or more precisely to generate a preferred temperature distribution within the mouse. A four channels optic fiber based thermometer (FOT Lab kit, Luxtron) can be employed to monitor the temperature of the mouse, which can be fed back to the heating module for control. This heating system can be readily adapted into a MBT system by adding an inlet and an outlet in a slightly larger mouse holder to facilitate airflow. Clearly, this setup could produce little obstruction in the optical paths. During the acquisition of these two datasets, the overall brightness of the mouse will be monitored to distinguish the signal changes due to the signal decay and the temperature increment. In addition to the gas-based simple heating method, other attractive heating techniques are also being explored, such as ultrasound and microwave heating.

4.3. Temperature mapping with micro-MRI

The temperature distribution within a mouse depends on the external temperature field, the mouse anatomy and physiology. Hence, it is difficult to compute. To make a full use of temperature-modulated datasets described above, the empirical relationship can be found between the temperature distribution within a mouse and the external temperature field using quantitative MRI thermometry based on the proton resonance frequency (PRF) (62). Note that absolute temperature measurement can be made using spectroscopic imaging based on proton chemical shift (CSI) to eliminate errors from the PRF method (63, 64). A mouse should be put in a standard posture within the mouse holder. Then, the 3D temperature map can be imaged within the mouse as a function of the external temperature field indicated by the temperature of the airflow. The resultant temperature distribution can be directly used to enhance the MBT reconstruction. Alternatively, an electronic atlas of the temperature distributions within a standard mouse may be constructed as a function of the external temperature field. In each MBT experiment, such an atlas is deformed according to the external temperature field for a temperature-modulated MBT reconstruction without using MRI thermometry. Clearly, the MRI based approach is theoretically desirable but the atlas-based method is practically cost-effective. These methods shall be evaluated to test the hypothesis in numerical simulation and phantom experiments that the atlas-based method would significantly improve the MBT results, and produce results similar to that obtained using the MRI based approach.

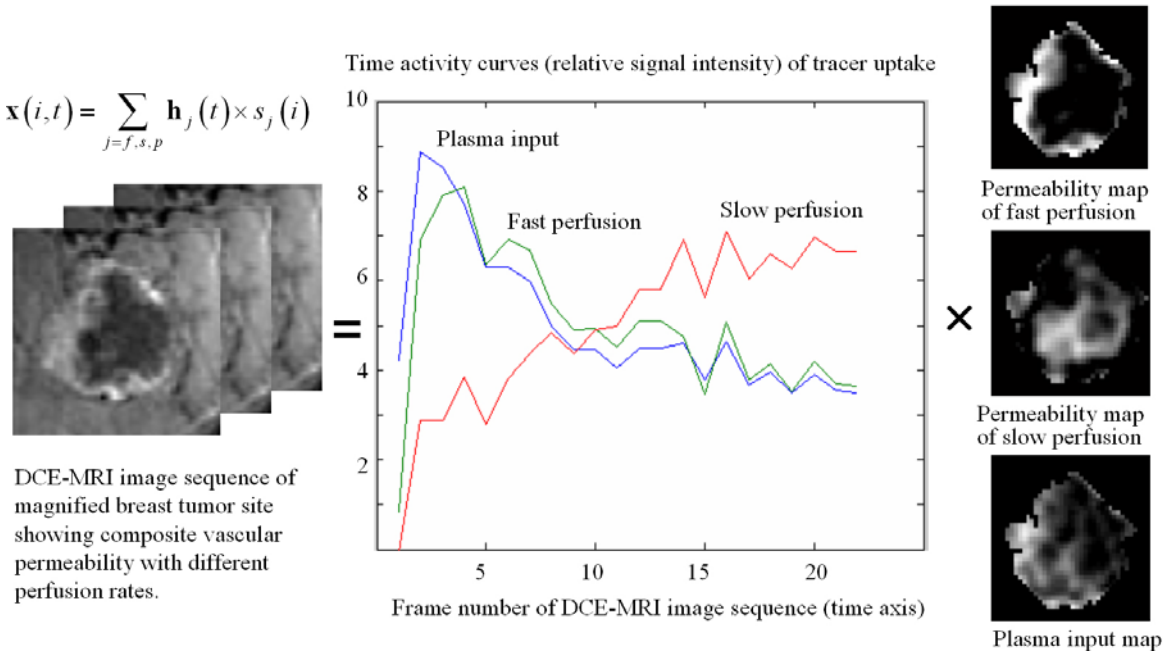

Figure 6. Application of the nLCA method for separating imagery mixtures in dual-energy x-ray lung scans (up-row image pair) into bone and tissue (bottom-row). The up-right panel is the scatter plot of mixed observations (correlated, low entropy), and the bottom-right is the scatter plot of unmixed source patterns.

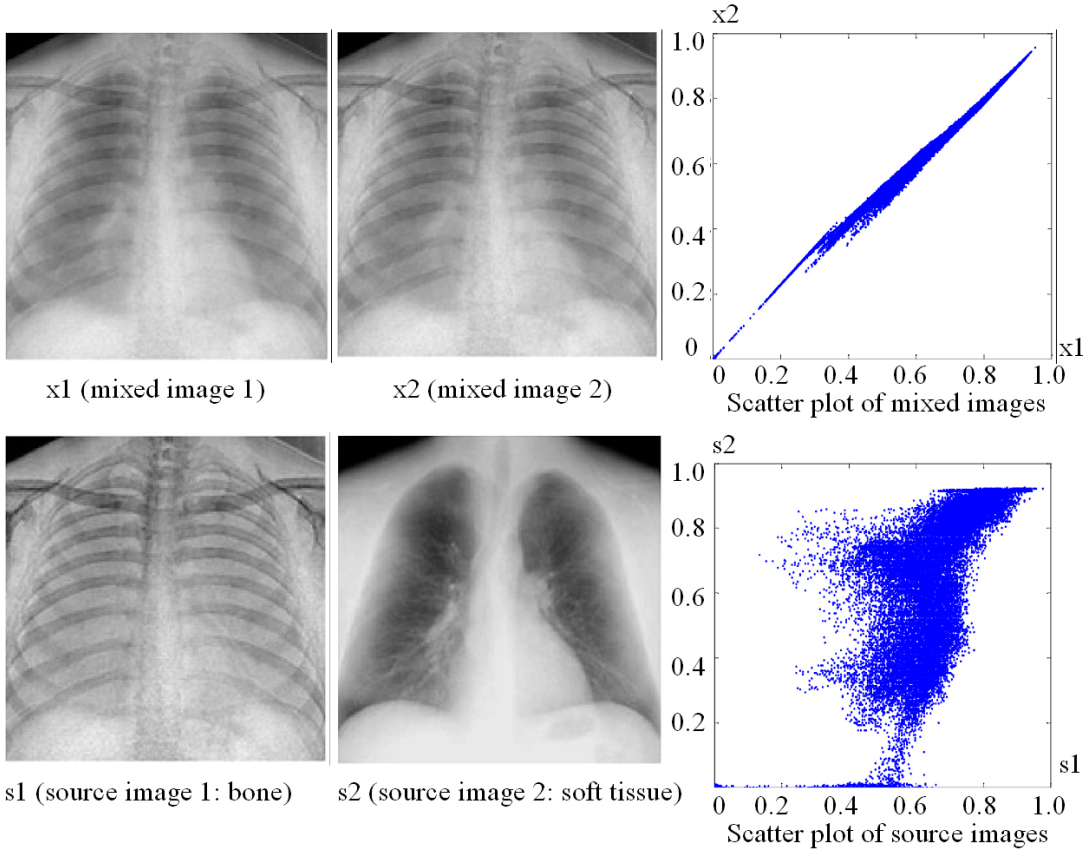

Figure 7. Bioluminescent intensity changes at (a) 24°C and (b) 37°C.

4.4. Temperature-modulated reconstruction

As an important application and a good starting point, let us first consider use of one bioluminescent probe. In a temperature-modulated bioluminescence imaging experiment, we will collect two bioluminescent datasets at base and elevated mouse body temperatures T_1 (for example, 25°C) and T_2 (for example, 37°C). Accordingly, the forward model is formulated as the following two linear systems

$$\left\{\tilde{\Phi}\left(T_l,\lambda_k\right)\right\}=\left[\mathrm{A}\left(\lambda_k\right)\right]\left\{S*\tilde{r}(T_l)\right\},\ k=1,2,...,N;\quad l=1,2 \tag{3}$$

where $\tilde{\Phi}(T_l,\lambda_k)$ is the measured photon fluence rate on the body surface of a mouse at a temperature T_l and a spectral bin center λ_k, $S*\tilde{r}(T_l)$ defined as $S_i\times\tilde{r}_i(T_l)$ for its ith element, S_i the source power at the base temperature, and $\tilde{r}_i(T_l)$ the ratio between the source power at T_l and that at T_1. The ratio distribution $\tilde{r}(T_2)$ can be estimated within the mouse body based on the MRI-based temperature distribution within the mouse and the *in vitro* temperature-dependent spectra of the bioluminescent probes (60) but they may be subject to errors under *in vivo* conditions. Since the temperature distribution is not uniform, by controlling the mouse to two biocompatible temperatures more information can be extracted from the measurement for superior MBT reconstruction. Therefore, the temperature-modulated MBT reconstruction can be performed by minimizing the objective function:

$$\min_{\substack{0\le S\le U\\ 0\le r(T)}}\left(\sum_{l=1}^{2}\left[\left\|\left\{\tilde{\Phi}(T_l,\lambda_k)\right\}-[\mathrm{A}(\lambda_k)]\{S*r(T_l)\}\right\|^2+\varepsilon\left\|r(T_l)-\tilde{r}(T_l)\right\|^2\right]+\lambda\eta(S)\right) \tag{4}$$

A modified Newton method with simple constrains and an active set strategy will be applied for the optimization.

Strictly speaking, the bioluminescent signal is not constant during two data acquisition processes. Hence, in the second dataset collected at the elevated temperature the signal increment due to the temperature elevation must be separated from the signal change due to the probe dynamics (signal rising, stabilized and decaying). Actually, in the first data acquisition session the probe dynamics can be analyzed to make a prediction using the traditional techniques. Then, in the second data acquisition session the difference can be quantified between the predicted signal intensity (at the base temperature) and the measure signal intensity (at the elevated temperature), which should be due to the temperature change. After preprocessing of the second dataset, the formulation given in the above paragraph can be applied directly. In the case of multiple bioluminescent probes inside a mouse, the above formulation can be extended but more steps will be involved.

5. DISCUSSIONS AND CONCLUSION

Based on the results and experience of ours and other leading groups, we envision that the emergence of the techniques described here will enable and facilitate new approaches to questions related to normal and disease biology using mouse models. With such capabilities, possibilities in facilitating biomedical studies would be numerous from molecular all the way to system levels. MBT alone or combined with other imaging modalities will allow the simultaneous evaluation of different markers related to a disease process with tomographic resolution in living mice. As this applies to the drug development, these methods could facilitate pharmacodynamic studies where one reporter provides information about the effect of the drug on the target and others relate target engagement to associated biologic processes such as cell proliferation or cell death (65, 66). Such information could be tremendously useful for both preclinical drug development which relies heavily on evaluating agents in mice to establish efficacy, toxicity and mechanism-of-action. One current limitation of this approach is the small number of bioluminescent enzymes and their available substrates offer few practical combinatorial possibilities for multispectral readouts. However, this limitation will be overcome when more probes become available and more modalities are combined with BLT.

In conclusion, we have reviewed on bioluminescence tomography, elaborated on its multi-spectral extension, described associated image unmixing and normalization techniques, and discussed a number of directions for technical improvements and biomedical applications. There are still major research opportunities ahead. Overall, we believe that bioluminescence tomography would eventually grow into a major optical molecular imaging modality, not only academically challenging and interesting but also practically valuable and instrumental in the development of the modern medicine.

7. ACKNOWLEDGMENT

This work was supported by grants from the National Institutes of Health (EB001685, EB002667, and EB000830), and by a grant from Department of Radiology, Univ. of Iowa, for development of micro-CT and bioluminescence tomography. We are grateful for insightful comments from Dr. Vasilis Ntziachristos with Harvard University, advice on MRI temperature mapping from Daniel Thedens with University of Iowa and Jianming Zhu with Wake Forest University, as well as input from others, all of which have helped significantly improve the quality of this overview.

8. REFERENCES

1. Zerhouni, E., Medicine: The NIH Roadmap. *Science*, 302(5642), 63-72, (2003)
2. Weissleder, R. and V. Ntziachristos: Shedding light onto live molecular targets. *Nature Medicine*, 9(1), 123-128, (2003)
3. Jaffer, F.A. and R. Weissleder: Molecular imaging in the clinical arena. *Jama*, 293(7), 855-862, (2005)
4. Thakur, M. and B.C. Lentle: Report of a summit on molecular imaging. *AJR Am J Roentgenol*, 186(2), 297-9, (2006)

5. Rice, B.W., M.D. Cable, and M.B. Nelson: In vivo imaging of light-emitting probes. *J. Biomed. Optics*, 6(4), 432–440, (2001)
6. Contag, C.H. and B.D. Ross: It's not just about anatomy: In vivo bioluminescence imaging as an eyepiece into biology. *J. Magn.Resonance*, 16(4), 378-387, (2002)
7. Minet, O.: The medical use of rescaling procedures in optical biopsy and optical molecular imaging. *Journal of Fluorescence*, 12(2), 201-204, (2002)
8. Choy, G., P. Choyke, and S.K. Libutti: Current advances in molecular imaging: Noninvasive in vivo bioluminescent and fluorescent optical imaging in cancer research. *Mol. Imaging*, 2(4), 303-312, (2003)
9. McCaffrey, A., M.A. Kay, and C.H. Contag: Advancing molecular therapies through in vivo bioluminescent imaging. *Mol. Imaging*, 2(2), 75-86, (2003)
10. Allemann, K.: Positron emission tomography: diagnostic imaging on a molecular level. *Schweiz Arch Tierheilkd*, 146(8), 359-64, (2004)
11. Pirko, I.: Magnetic resonance imaging, microscopy, and spectroscopy of the central nervous system in experimental animals. *NeuroRx*, 2(2), 250-64, (2005)
12. Apisarnthanarax, S. and K.S. Chao: Current imaging paradigms in radiation oncology. *Radiat Res*, 163(1), 1-25, (2005)
13. Dobrucki, L.W. and A.J. Sinusas: Molecular imaging. A new approach to nuclear cardiology. *Q. J. Nucl. Med. Mol. Imaging*, 49(1), 106-15, (2005)
14. Peremans, K.: A review of small animal imaging planar and pinhole spect Gamma camera imaging. *Vet. Radiol. Ultrasound*, 46(2), 162-70, (2005)
15. Niziachristos, V.: Fluorescence molecular tomography resolves protease activity in vivo. *Nature Medicine*, 8(7), 757-761, (2002)
16. Cong, A. and G. Wang: A finite-element-based reconstruction method for 3D fluorescence tomography. *Optics Express*, 13(24, 9847-9857, (2005)
17. Wang, G., Y. Li, and M. Jiang: Uniqueness theorems in bioluminescence tomography. *Med. Physics*, 31(8), 2289-2299, (2004)
18. Wang, G.: Development of the first bioluminescent CT scanner. *Radiology*, 229(P), 566, (2003)
19. Cong, W.X.: Practical reconstruction method for bioluminescence tomography. *Optics Express*, 13(18), 6756-6771, (2005)
20. Cong, W.X. and G. Wang: The boundary integral method and Apparatus for bioluminescence tomography. 2005, Patent disclosure filled with Univ. of Iowa Research Foundation in December 2005, UI#06038: USA.
21. Jiang, M. and G. Wang: Methods and apparatus for bioluminescence tomography from partial measured data. 2006, Patent disclosure filled with Univ. of Iowa Research Foundation in February 2006, UI#06051: USA.
22. Wang, G.: Multi-spectral bioluminescence tomography methods and systems. 2004, Patent disclosure filled with Univ. of Iowa Research Foundation in April 2004, UI#04070; US Provisional Patent Application filed on January 3, 2006 (60/756, 036): USA.
23. Wang, G.: Optical molecular tomography systems and methods for simultaneous acquisition of multi-view and multi-spectral data. Patent disclosure filled with Univ. of Iowa Research Foundation in May 2006, UI#06079: USA. (2006)
24. Wang, G.: Dynamic bioluminescence tomography method and apparatus. 2004, Patent disclosure filled with Univ. of Iowa Research Foundation in December 2004, UI#05039: USA. (2004)
25. Wang, G.: Temperature-modulated bioluminescence tomography. 2006, Patent disclosure filled with Univ. of Iowa Research Foundation in May 2006, UI#06080: USA. (2006)
26. Wang, G.: Development of the first bioluminescent CT scanner. *RSNA' 03*, Chicago, (2003)
27. Bräuer, R.: Measuring luminescence with a low light level imaging system using electronic light standards. *Bioluminescence and Chemiluminescence status report*, 13-17, (1993)
28. Berthold, E.G., Luminograph LB 980 product brochure. (1992)
29. Hamamatsu, Argus-50 product brochure. (1995)
30. Stanley, P.E.: A survey of more than 90 commercially available luminometers and imaging devices for low light measurements of chemiluminescence and bioluminescence, including instruments for manual, automatic and specialized operation, for HPLC, LC, GLC and microtitre plates. Part 1: Descriptions. *J. Biolumin. Chemilumin.*, 7, 77-108, (1992)
31. Stanley, P.E.: Commercially available luminometers and imaging devices for low-light measurements and kits and reagents utilizing chemiluminescence or bioluminescencc: Survey Update 1. *J. Biolumin. Chemilumin.*, 8, 273-240, (1993)
32. Stanley, P.E.: Commercially available luminometers and imaging devices for low-light measurements and kits and reagents utilizing chemiluminescence or bioluminescence: Survey Update 2. *J. Biolumin. Chemilumin.*, 9, 51-53, (1994)
33. Stanley, P.E.: Commercially available luminometers and imaging devices for low-light measurements and kits and reagents utilizing chemiluminescence or bioluminescence: Survey Update 3. *J. Biolumin. Chemilumin.*, 9, 5123-5125, (1994)
34. Contag, C.H. and M.H. Bachmann: Advances in In vivo bioluminescence imaging of gene expression. *Annu. Rev. Biomed. Eng*., 4, 235-260, (2002)
35. Contag, C.H. and P.R. Contag: Viewing disease progression through a bioluminescent window. *Optics and Photonics News*, 7(1), 22-23, (1996)
36. Contag, C.H.: Visualizing gene expression in living mammals using a bioluminescent reporter. *Photochem. Photobiol.*, 66(4), 523-531, (1997)
37. Qian, X.: Bioluminescent Source Estimation Using Computational Optical Biopsy in Liposyn-10%. *Appl. Optics*, (Appear 2007)
38. Shen, H.: Numerical study on the validity of the diffusion approximation for computational optical biopsy. *J. OSA A-Opt. Image Sci. and Visi.*, 24(2), 423-429, (2007)
39. Coguos, O.: Determination of depth of in-vivo bioluminescent signals using spectral imaging techniques. in Genetically Engineered and Optical Probes for Biomedical Applications. *San Diego: SPIE*, (2003)
40. Kuo, C., H. Xu, and B. Rice: Improved techniques in diffuse luminescent tomography on whole animal meshes. *SMI 2006*, Hawaii. (2006)

41. Wang, G., E.A. Hoffman, and G. McLennan: Systems and methods for bioluminescent computed tomographic reconstruction. 2002, Patent disclosure filled with Univ. of Iowa Research Foundation in July 2002; US provisional patent application filled in March 2003; US patent application filed in March 2004: USA.
42. Cong, W.X. and G. Wang: Boundary integral method for bioluminescence tomography. *J. Biomed. Optics*, 11(2), 020503-1, (2006)
43. Jiang, M. and G. Wang: Image reconstruction for bioluminescence tomography. *Proceedings of SPIE, Society of Photo-Optical Instrumentation Engineers*, Bellingham, WA, USA, (2004)
44. Gu, X.: Three-dimensional bioluminescence tomography with model based reconstruction. *Optics Express*, 12, 3996-4000, (2004)
45. Cong, W.X.: In vivo tomographic imaging based on bioluminescence. *Proceedings of SPIE, Society of Photo-Optical Instrumentation Engineers*, Bellingham, WA, USA, (2004)
46. Chaudhari, A.J.: Hyperspectral and multispectral bioluminescence optical tomography for small animal imaging. *Phys. Med. Biol.*, 50, 5421-5441, (2005)
47. Dehghani, H.: Spectrally-resolved bioluminescence optical tomography. *Optics letter*, 31(3): p. 365-367, (2006)
48. Cong, W.X.: A Born-type approximation method for bioluminescence tomography. *Medi. Physics*, 33(3), 679-686, (2006)
49. Kuo, C.: Bioluminescent tomography for in vivo localization and quantification of luminescent sources from a multiple-view imaging system. *Mole. Imaging*, 4(370), (2005)
50. Wang, G.: In vivo mouse studies with bioluminescence tomography. *Optics Express*, 14(17), 7801-7809, (2006)
51. Cong, A. and G. Wang: Multi-spectral bioluminescence tomography: Methodology and simulation. *Int'l J.of Biome*d. *Imaging*, ID57614, 1-7, (2006)
52. Han, W., W.X. Cong, and G. Wang: Mathematical study and numerical simulation of multispectral bioluminescence tomography. *Int'l J.of Biome*d. *Imaging*, (2006)
53 Alexandrakis, G., F.R. Rannou, and A.F. Chatziioannou: 3D bioluminescence imaging by use of a combined optical-PET tomographic system: A computer simulation feasibility study. *Phys. Med. Biol*., 50, 4225-4241, (2005)
54. Herschman, H.R.: Molecular imaging: Looking at problems, seeing solutions. *Science*, 302(5645), 605-608, (2003)
55. Keshava, N. and J.F. Mustard: Spectral unmixing. *IEEE Sign. Proc. Magazine*, 19(1), 44-57, (2002)
56. Mansfield, J.R., C.A. Kerfoot, and R.M. Levenson: Multiplexing molecular markers with multispectral imaging. *Proc.on the nexus of histochemistry and mole. Genetics*, Hawaii, (2006)
57. Corlu, A.: Uniqueness and wavelength optimization in continuous-wave multispectral diffuse optical tomography. *Optics Letter*, 28, 2339-2341, (2003)
58. Arridge, S.R.: A finite-element approach for modeling photon transport in tissue. *Med. Physics*, 20(2), 299-309, (1993)
59. Liu, Y., L.Z. Sun, and G. Wang: Tomography-based 3-D anisotropic elastography using boundary measurements. *IEEE Trans. on Med. Imaging*, 24(10), 1323-1333, (2005)
60. Zhao, H.: Emission spectra of bioluminescent reporters and interaction with mammalian tissue determine the sensitivity of detection in vivo. *J. Biomed. Optics*, 10(4), 041210, (2005)
61. Wang, G.: Temperature-modulated bioluminescence tomography. *Optics Express*, 14(7), 7852-7871, (2006)
62. Quesson, B., J.A.d. Zwart, and C.T. Moonen: Magnetic resonance temperature imaging for guidance of thermotherapy. *J. Magn. Reson. Imaging*, 12, 525-533, (2000)
63. Ishihara, Y.: A precise and fast temperature mapping using water proton chemical shift. *Magn. Reson. Med.*, 34, 814-823, (1995)
64. Poorter, J.D.: Noninvasive MRI thermometry with the proton resonance frequency (PRF) method: in vivo results in human muscle. *Magn. Reson. Med.*, 33, 74-81, (1995)
65. Laxman, B.: Noninvasive real-time imaging of apoptosis. *Proc. Nali. Acad. of Sci. USA*, 99(26), 16551-16555, (2002)
66. Gross, S. and D. Piwnica-Worms: Monitoring proteasome activity in cellulo and in living animals by bioluminescent imaging: Technical considerations for design and use of genetically encoded reporters. *Methods in Enzymology*, 399, 512-530, (2005)
67. Wang, Y., J. Zhang, and K. Huang: Independent component imaging of disease signatures. *IEEE International Symposium on Biomedical Imaging*, Washington, DC, (2002)
68. Wang, Y., R. Srikanchana, and P. Choyke: Computed simultaneous imaging of multiple functional biomarkers. *IEEE International Symposium on Biomedical Imaging*, Arlington, VA, (2004)
69. Wang, Y.: Modeling and Reconstruction of Mixed Functional and Molecular Patterns. *IJBI*, 29707-9, (2006)
70. Chen, S., C.A. Bouman, and M.J. Lowe: Clustered component analysis for functional MRI. *IEEE Trans. on Med. Imaging*, 23(1), 85-98, (2004)
71. Wang, Z.: Optimized multilayer perceptrons for molecular classification and diagnosis using genomic data. *Bioinformatics*, 22(6), 755-761, (2006)
72. Oja, E. and M. Plumbley: Blind separation of positive sources by globally convergent gradient search. *Neural Computation*, 16(9), 1811-1825, (2004)
73. Martinez-Zaguilan, R., L.S. Tompins, and R.M. Lynch: Simultaneous analysis of multiple fluorescent probes in single cells by microscopic imaging. *Proc. SPIE: Time-Resolved Laser Spectroscopy in Biochemistry*, Los Angeles, (1994)
74. Eckstein, J.W.: A time-dependent bacterial bioluminescence emission spectrum in an in vitro single turnover system: Energy transfer alone cannot account for the yellow emission of Vibrio fischeri Y-1. *Proc. Natl. Acad. Sci. USA.*, 87, 1466-1470, (1990)
75. Gast, R. and J. Lee: Isolation of the in vivo emitter in bacterial bioluminescence. *Proc. Natl. Acad. Sci. USA.*, 75(2), 833-837, (1978)
76. Howland, P. and H. Park: Generalizing discriminant analysis using the generalized singular value

decomposition. *IEEE Trans. on Pattern Analysis and Machine Intelligence*, 26(8), 995-1006, (2004)
77. Van Loan, C.F.: Generalizing the singular value decomposition. *SIAM J. of Nume. Analysis*, 13(1), 76-83, (1976)
78. Wang, Y.: Probabilistic principal component subspaces: a hierarchical finite mixture model for data visualization. *IEEE Trans. on Neural Networks*, 11(3), 625-636, (2000)
79. Wang, Y.: Independent component imaging, 396, (2004)

Key Words: Tomography, Bioluminescence, Imaging, Review

Send correspondence to: Professor Ge Wang, Bioluminescence Tomography, Laboratory, Department of Radiology, University of Iowa, 200 Hawkins Drive, Iowa City, IA 52242, USA, E-mail: ge-wang@ieee.org

http://www.bioscience.org/current/vol13.htm